

Determination of the coordinates of a circle using distributed fibre-optic length changes

Eike BARNEFSKE^{1,*}, Clemens SEMMELROTH², Annette SCHEIDER², and Harald STERNBERG²

¹ Bundesgesellschaft für Endlagerung mbH, Peine, Germany, (eike.barnefske@bge.de)

²HafenCity Universität Hamburg, Hamburg, Germany, (clemens.semmelroth@hcu-hamburg.de, annette.scheider@hcu-hamburg.de, harald.sternberg@hcu-hamburg.de)

* corresponding author

Abstract

Distributed fiber optic sensors (DFOS) are used to determine the deformation of engineering structures (objects). This measurement method analyzes changes in the backscatter signal along a fiber in order to determine changes in length and/or temperature. Various analytical and setup procedures make it possible to separate thermal and mechanical influences affecting the fiber. The geometric object changes can be directly derived as strain. The information of strain is not sufficient for a number of object state descriptions, so that further variables, such as inclinations, curvatures and coordinates, must be derived. In order to determine these variables, several fibers are often installed in a suitable geometric arrangement along the deformation directions. For example, a curvature can be determined from two fibers running parallel at a known distance. Deriving coordinates from curvatures or other intermediate values is much more complex and uncertain. This work focuses on the derivation of coordinates and coordinate changes for circular or elliptical objects (e.g. boreholes, tunnels or shafts) by means of length change measurements. Two approaches are evaluated in which some of the geometric constraints can be controlled. On the one hand, a popular approach using an adjustment of local circles is evaluated. On the other hand, an approach based on divided lines and a line network adjustment is developed. A highly precise test data set is created for the development and evaluation of the methods. The test dataset consists of DFOS, laser tracker and photogrammetric measurements of a test object in different deformation states.

Keywords: distributed fiber optic sensors, deformation monitoring, adjustment calculation

Received: 2nd December 2024. Revised: 11th February 2025. Accepted: 25th February 2025.

1 Introduction

Distributed fiber optic sensors (DFOS) enhance the traditional geodetic, mining surveying and geotechnical measuring systems that are used to determine geometric changes of an object. Fibers as sensors can be installed in soil and constructions with low effort. The main advantages of DFOS are the high local density of measured values, the low set-up effort for subsequent measurements, the high precision and reliability of the strain measurement (relative) and the capability of installing the sensors in existing constructions. To determine geometric changes with the fiber, primarily the strain along the fiber is used. By arranging the fiber in specific configurations and measuring the fibers position, posi-

tion and height changes as well as object deformations can be determined in an evaluation process. Applications for DFOS with such following evaluations include the monitoring of dams and landfills (Döring et al., 2016), the monitoring of bored piles (Franz et al., 2023) or the monitoring of tunnel structures (Monsberger et al., 2022). From these applications it becomes clear that strain alone is not sufficient for an effective description and evaluation of the object condition, so that coordinate changes (polar and cartesian) must be determined. In this paper, two central evaluation approaches are considered (section 4) and evaluated in a laboratory experiment (section 3). The second method is to our knowledge novel and can simplify the evaluation for geotechnical applications (section 4.2). The results

of the experiment and the challenges that arise in object monitoring are discussed (section 5).

2 State of the art

The initial developments in DFOS were driven by the emergence of lasers and optical fibers in the 1960s and 1970s (Hartog, 2017). The DFOS technology enables target-oriented and locally high-resolution monitoring of deformation in the construction and operational phases of tunnels, mines, walls, dams and bridges (Minardo et al., 2012; Lopez-Higuera et al., 2011; Ye et al., 2014).

2.1 DFOS Principle

The specific physical phenomenon employed to determine object deformations based on strains in optical fibers varies depending on the distributed fiber optic sensor in use. However, all distributed fiber optic sensors utilize the scattering effects of light that is penetrated into the optical fiber. The back-scattered or phase-shifted light from the interaction with fiber is then analyzed. Three distinct types of light scattering or phase-shifted methods are employed in DFOS, namely Rayleigh, Raman and Brillouin. The latter DFOS sensing principle is employed in the present study using Brillouin optical frequency domain analysis (BOFDA). Laser light is coupled into the fiber from both ends with the objective of detecting the specific Brillouin frequencies at which the light wave stimulates the fiber at an acoustic level (Hartog, 2017; Nöther, 2010). The Brillouin frequency shift is then used to derive either the temperature or/and the strain at every location in the fiber.

2.2 Application and approaches for deformation monitoring in mines or tunnels

With respect to the application of DFOS in mining, a number of studies have addressed the monitoring of surface mines, including different geological strata of coal mines (Cheng et al., 2015; Hu et al., 2020; Xie et al., 2023). In underground mining, Naruse et al. (2007) have presented an underground monitoring system based on DFOS to detect the deformation of gallerias. To the present day field research in underground mines is ongoing, e.g. to show the economic use of temperature and strain monitoring during mining activities (John

and Hoehn, 2024). In all cases BOFDR has been employed to monitor the stability of the structures.

Since the 2010s, fiber optic sensors have also been used in tunnels to assess the structural integrity of the latest exceptionally long traffic tunnel projects. For instance with Fiber Bragg Gratings Sensors (de Battista et al., 2015; Henzinger et al., 2018) and later with Brillouin and Rayleigh-based Sensors (Monsberger and Lienhart, 2021) in a tunnel cross-section. Based on the strain measurements mathematical approaches to describe the deformation are developed. This approach of complex evaluation to determine indirect target variables (position changes of points or radial changes) forms the focus of this paper.

3 Experiment and reference methods

The aim of the experiment is to evaluate the suitability of the DFOS measuring system and the evaluation methods for determining the deformation of circular objects. In a down-scaled laboratory experiment the deformation of a Hula hoop can be caused and determined at the two points where the anchors pull or push. This deformation corresponds to the distance moved and adjusted by the anchors. The deformation at all other points of the hoop can only be determined using another measuring system. Photogrammetric measuring systems, coordinate measuring machines, articulated measuring arm or laser trackers with and without precision laser scanners are suitable for this measurement, because of their reliable, precise and locally high-resolution measurement readings. The experimental setup is briefly explained in section 3.1. The implementation and evaluation of the two reference measurements are outlined in sections 3.2 and 3.3.

3.1 Experimental setup

The plastic Hula hoop with a diameter of 0.8 m (circumference approx. 2.54 m) serves as the test object, which can be deformed in a test rig along an axis based on fix parameters. In the test rig, the hoop can be pulled or pushed at two points (Figure 1). The tension resp. compression points are opposite each other so that the axes of the main deformation (axis across these points and orthogonal to this axis) are known. Each anchor point is moved

in several epochs in 5 mm or 10 mm steps so that a uniform strain should occur. The maximum deformation of the hoop in the main axis is 90 mm, so the maximal diameter is 0.890 m and the minimal diameter is 0.710 m.

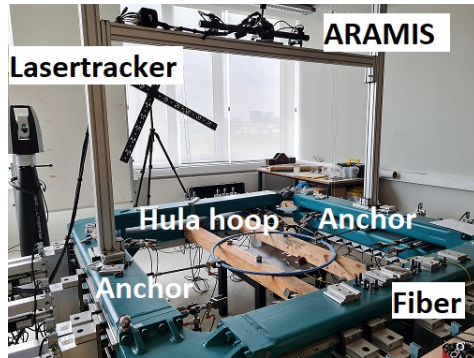


Figure 1. Experimental setup: Instruments, Hula hoop (test object) and test rig.

The reference measurements provide the target deformation of the hoop as a continuous point cloud and as discrete surface points. The radial deformation is derived from the point cloud or the coordinates. Due to the experimental setup, only deformations of the hoop in the plane (x- and y-axes) were observed in the reference data.

The DFOS measurement is carried out with the interrogator *ftB 5020* using the BOFDA-mode, which has a minimal spatial resolution of 0.2 m (special mode) or 0.5 m and records strain with an accuracy of around $2 \mu\text{m}/\text{m}$ (2σ) (fibrisTerre Systems GmbH, 2020). The bare single mode Corning Ultra fiber is installed inside and outside the hoop by the SikaFast 555L05 two-component adhesive (Figure 2).

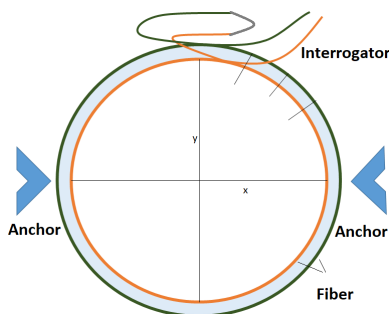


Figure 2. Hula hoop with installed fiber to measure the strains and compressions inside and on the outer edge. Anchors 1 and 2 can be moved.

3.2 Photogrammetric measuring system

The photogrammetric measuring system (ARAMIS) used enables the highly accurate and kinematic recording of strains and position changes in a small measurement volume under controllable environmental conditions. For this purpose, either discrete targets or prominent points are tracked in a stochastic pattern on the measurement object surface over the experiment period. Position changes or the new positions are determined by the static stereo camera system so that very high temporal resolution monitoring is possible. The positions of the discrete target points in relation to the initial position and the defined coordinate system were primarily determined in five static epochs. The practical accuracy for position change was estimated to be less than 0.1 mm in the experiment.

3.3 Lasertracker

A three-dimensional point cloud of the hoop can be measured by means of the AS1 handheld scanner and the AT960 LR laser tracker for each epoch. The accuracy of the points is estimate with 0.1 mm (2σ). The point cloud is referenced to the center of the initial circle center point. The distances between points on the hoop edge and the center point can be determined after manually cleaning the point cloud. The distance for an edge point to the center point is the local or segment radius. For the evaluation, one point for each segment is determined.

4 Methods of deformation parameter analysis

The aim of the following evaluation methods is to determine the change in the local radii and the coordinate displacement of points on the circumference from the strain and compression measurements with DFOS. These parameters are established for the description of the deformation of circular objects and can be determined directly using the measurement techniques (section 3) and the evaluation methods described in sections 4.1 and 4.2. Two central approaches are described in the literature for the determination of radial changes and the coordinate displacement of circumferential points. The first approach involves calculating curvatures from several fiber cables that run parallel in a circle. The curvatures are then the basis for calculating the radial

changes or the point displacements in an adjustment (Monsberger and Lienhart, 2021; Pei et al., 2013). The local curvatures can also be used for the direct determination of local radii (section 4.1). The second approach uses a special fiber cable with a fixed block in which several fibers are embedded at fixed positions. The fixed distances between the fibers can be used to determine the changes in direction via trapezoids along the fiber (Bednarz et al., 2021). Due to the large cable, this approach cannot be used in the experiment and is not considered in more detail. An approach for determining the parameters with only one fiber per cable using the local circumferential change directly is presented in sections 4.2.

4.1 Curvature-based method

Fibers can primarily be used to measure changes along the laying axis. If two or more fibers run parallel and their distance is precisely known, then the strain measurement can be used to determine a change orthogonal to the axis of the fiber course. This can be applied in two applications as shown in Figure 3. If the fibers are run in a straight line, the inclination of the axis parallel to the fibers can be determined after integration with calculated distances (Figures 3 a and b).

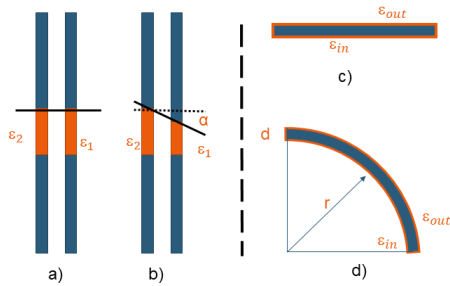


Figure 3. Inclination calculation with two parallel fibers. a) State with no inclination. b) Inclination state expressed by an inclined plane. Strong curvature at the quarter circle. c) Straight object. d) Curved object. Determination of the radius of curvature from elongation and shortening at the inner and outer edge.

With the two parallel fibers, also the curvature can be derived from the changes of the circumferential segments. Figures 3c and d illustrate how the linear relationship between radius r and circumference exists. The principle can be illustrated using the example of bending a straight. The outer side of the

pipe is lengthened and the inner side is shortened in the same way. The bending radius is determined by the strain (outside), the compression (inside), the original pipe length and the diameter. Equation 1 can be used to calculate the local curvature κ for each segment s (Monsberger and Lienhart, 2021).

$$\kappa(s) = \frac{1}{r(s)} = \frac{\epsilon_{out}(s) - \epsilon_{in}(s)}{d(s)} \quad (1)$$

The distance between the fibers d must be known. The distance and the segment size (area over which the strain is measured) are further parameters that influence the quality of the curvature calculation and must be determined as precisely as possible. The smaller the segment, the more directly the deformation can be represented. Influences of longitudinal stress are compensated for by applying the mean strain from equation 2. The segment curvature $\kappa(s)$ can be calculated by equation 3 (Monsberger and Lienhart, 2021).

$$\bar{\epsilon}(s) = \frac{\epsilon_{out}(s) + \epsilon_{in}(s)}{2} \quad (2)$$

$$\kappa(s) = \frac{\epsilon_{out}(s) - \epsilon_{in}(s)}{d(s) * (1 - \bar{\epsilon}(s))} \quad (3)$$

Equation 4 is used to calculate the local change in curvature $\delta\kappa$ along the circumference of the circle. The initial curvature of the circle $\kappa_{Initial}$ cannot be detected directly by the fiber. As described in section 3.3, a laser scan can be used to derive the local radii for any segment and determine the local curvatures. A local radius can then be calculated for each location on the circumference using the initial curvature and the curvature changes according to equation 5. This radius does not take into account the influences of the neighborhood. In addition, incorrect measurements are not detected with this purely numerical solution.

$$\delta\kappa(s) = \frac{1}{\delta r(s)} \quad (4)$$

$$r(s) = \frac{1}{\delta\kappa(s)} + \frac{1}{\kappa_{Initial}(s)} \quad (5)$$

A more reliable evaluation is provided by the segment curvature approach described in Monsberger

and Lienhart (2021); Monsberger et al. (2022) using double integration in an adjustment model. For this approach, the three segment radii w of a curvature segment with width h are calculated according to equation 6. This approach requires a solid knowledge of the stochastic model for all the parameters mentioned above and knowledge of absolute or initial states.

$$\kappa_i = \frac{1}{h^2} * (w_{i+1} - 2 * w_i + w_{i-1}) \quad (6)$$

4.2 Circumference change-based method

In many applications, the global circular deformation (e.g. towards an ellipse) is of primary interest, so that deformations can be represented by few points. With this prior knowledge about the interpretation of the measurement results and potential deformation trends, an efficient evaluation approach based on parameterizable geometries can be implemented. In a circle, the global deformation can be represented sufficiently well by eight points, so that an equilateral octagon is placed in the circle. The eight points create circumference sections B . In the deformation-free state, the points of the octagon lie on the circumference of the circle and the sides of the octagon are chords of the circle a_x . Further chords between every second point can be introduced into the model by two squares b_x . Finally, the diameters of the circle d_x are defined by these points. The complete network of lines is shown in Figure 4.

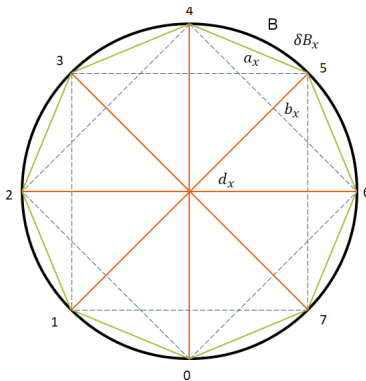


Figure 4. Circle with geometries to represent the geometric relationships.

By introducing the mesh of lines and the circumference points, circular deformations can be caused via

line changes, so that there is a relationship between changes in the circumference length and the line lengths. This relationship can be expressed by the equations 7 to 9. The sectional changes in the length of the circumference can be determined by integrating the strain measurements. With the change in length of the circumference sections δB , the chords can be calculated with equations 7 and 8 and the eight diagonals (diameters) with equation 9.

$$a_x = \frac{8 * (B - \delta B)}{\pi * \sqrt{4 + 2 * \sqrt{2}}} \quad (7)$$

$$b_x = \frac{(B - \delta B) * 2 * \sqrt{2}}{\pi} \quad (8)$$

$$d_x = \frac{(B - \delta B) * 2}{\pi} \quad (9)$$

The eight circumferential points are used to describe the deformation. Their approximately position is known from the geometry or can be roughly calculated using the *arc section* method, if the circular deformation has already progressed. With the redundant lines and the two-dimensional coordinates of the circumferential points, the final point coordinates can be determined in a *Gauss-Markov line mesh adjustment*. The results for a simulation are shown in Figure 5.

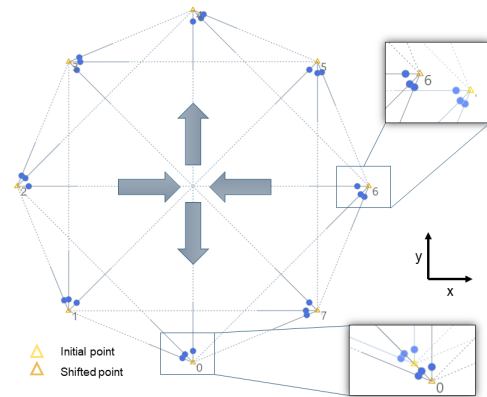


Figure 5. Adjusted mesh of a deformed circle with simulated data. A convergence is present in the x-axis. This leads to a divergence in the y-axis (created with JAG3D).

5 Results and Discussion

The presented methods can be used in theory to determine local radial changes and changes in the 2D

circumferential coordinates. In a simulation with discrete and locally high-resolution strain measurements, as well as the known position of the fiber, the mathematical relationship has been confirmed. A transfer of the methods to the measurement results of the experiment is possible with significant limitations. Central limitations arise due to the coarse local resolution, mixed strain measurements at the edges of the measurement sections, local stresses of the hoop, uncertainty in determining the fiber position and the interaction of the composite adhesive with the fiber and the hoop.

The first method (section 4.1) performs a curvature calculation for each segment in the first step. Since each segment must be 0.2 m long and the circumference is approximately 2.5 m (12.7 segments), the first and last segments will always contain strains of the feed fiber. The first and last segments therefore do not provide the true curvature or radius so that a ring closure is not possible (Figures 6 and 7).

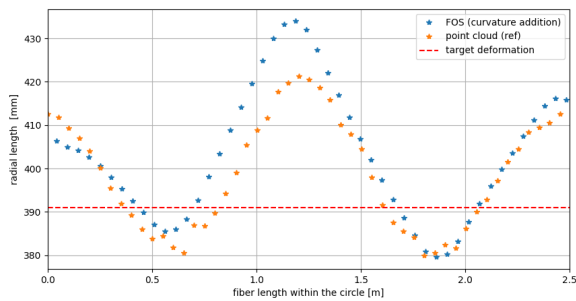


Figure 6. Radial changes at 17 mm push of each anchor.

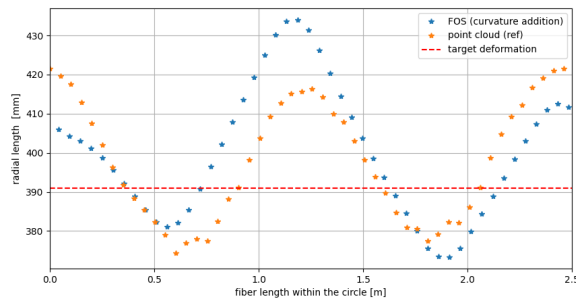


Figure 7. Radial changes at 22 mm push of each anchor.

Figures 6 and 7 show the local radii of each segment for epochs 4 and 5 compared to the corresponding radii calculated from the point cloud. It can be seen from these figures that there is a qual-

itative correlation between DFOS-derived radii and the radii determined from the point cloud. There is also a phase shift between FOS and reference values, which is probably caused by the low spatial resolution. This required the estimation of the radius for the first segment. The deviations between radii are primarily due to the coarse sampling of the strain measurement so that the radial change is amplified. Due to this uncertainty and indeterminacy, the adjustment model (step 2 of method 1) cannot return a plausible result. Adjustments that would make an evaluation possible would be to move the start segment to a deformation-free / low-deformation area so that initial curvatures can be estimated more accurately. An improvement in local resolution could be achieved by using a different measuring principle, e.g. Rayleigh method. An alternative would be to use it only at low strains so that the stochastic variables can be better estimated.

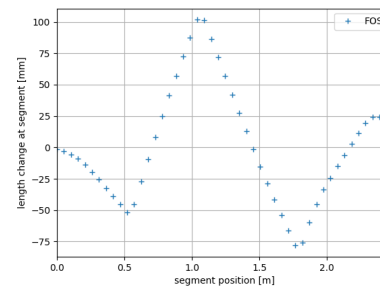


Figure 8. Change in length of the circumferential segments at 17 mm push of each anchor.

The second method is based on the change in length of the circumference in each segment. Each segment has a length of approximately 306 mm in the deformation-free state at eight support points and is formed by interpolation (mathematical increase in spatial resolution) and later addition of the interpolated segments. By integrating over the segment length, the segmental change in length can be determined. Only the inner fiber needs to be analyzed for this. Figure 8 shows that the change in length of the segments occurs as a dependency of the radial change. This observation leads to the conclusion that the changes in circumferential length lead to a displacement of the eight support points. According to section 4.2, the distances between the points are calculated from the arc segments and a distance adjustment is made. The deformation-free position of the points is used as an approximation. The result of the adjustment for the divergence case is shown

in Figure 9.

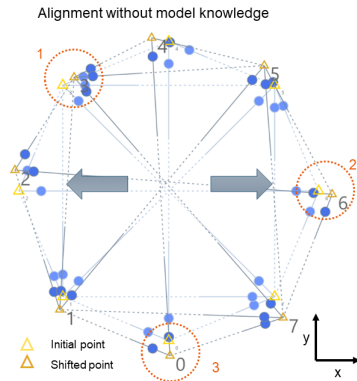


Figure 9. Result of the mesh adjustment without support. Marking 1: point in deformation-free zone. Markings 2 and 3: points in deformation zone (created with JAG3D).

The load case from the experiment shows that the hoop is pulled to the right and left so that stretching is expected in the x-direction. This expectation is not completely consistent with the result in Figure 9. Extensions are also recognized in the y- or xy-direction. This method cannot be used without supporting the model (a priori knowledge), as displacements from the circumference also act in the deformation-free area and thus lead to a reduction of the deformation in the actual deformation directions.

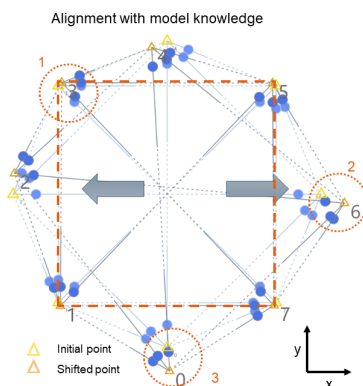


Figure 10. Result of the mesh adjustment with support. Marking 1: point in deformation-free zone. Markings 2 and 3: points in deformation zone (created with JAG3D).

The model can be supported by introducing additional distance measurements, as shown by the marked square in Figure 10. The deformation at marking 1 is reduced and leads to reinforcement at markings 2 and 3 (deformation areas). Remaining

deviations from the target position are due to the above-mentioned influences of strain measurement or result from an inaccurate alignment of the hoop.

6 Conclusion and outlook

Two methods for determining the coordinate displacements of the boundary points are introduced and analyzed in an experiment. Both methods are applicable with simulated data and with deformations of a hoop within one defined axis. The experiment shows that neither of these methods can be applied without significant limitations. Both methods can only be plausibly used to calculate the deformation parameters (boundary point coordinates and radial changes) for small deformations or when external constraints are introduced. In particular, the discretization of the start and end segments and the deformation of these segments can only be supported by external and absolute measurements (e.g. with total stations, distance sensors or extensometers). The central improvement is seen in the optimization of the stochastic model for method 1. For method 2, it is conceivable that the relationship between radius and circumference changes can be investigated in more detail. The experimental results demonstrate that in order to apply the methods to a real shaft, the position of the fiber must be known very precisely and the absolute deformations must be recorded with additional sensors or measurements so to enable a plausible calculation of deformation parameters. Method 1 assumes that two parallel fibers can be installed with a distance of several centimeters around the shaft. In practice, this is often not possible in existing structures. The longer circumference of the shaft means that only global deformations are detected with method 2.

Acknowledgements

Special thanks to Marcus Illguth, Alexandros Apostolou and Lennert van der Wall for their excellent support during the practical experiments.

References

Bednarz, B., Popielski, P., Sienko, R., Howiacki, T., and Bednarski, L. (2021). Distributed fibre optic sensing (DFOS) for deformation assessment

- of composite collectors and pipelines. *Sensors*, 21(17).
- Cheng, G., Shi, B., Zhu, H.-H., Zhang, C.-C., and Wu, J.-H. (2015). A field study on distributed fiber optic deformation monitoring of overlying strata during coal mining. *Journal of Civil Structural Health Monitoring*, 5(5):553–562.
- de Battista, N., Elshafie, M., Soga, K., Williamson, M., Hazelden, G., and Hsu, Y. S. (2015). Strain monitoring using embedded distributed fibre optic sensors in a sprayed concrete tunnel lining during the excavation of cross-passages. In de Stefano, A., editor, *7th International Conference on Structural Health Monitoring of Intelligent Infrastructure (SHMII 2015)*. Curran Associates Inc, Red Hook, NY.
- Döring, H., Habel, W., Lienhart, W., and Schwarz, W. (2016). Faseroptische Messverfahren. In *Handbuch der Geodäsie*, pages 1–48. Springer Berlin Heidelberg.
- fibrisTerre Systems GmbH (2020). Distributed fiber-optic brillouin sensing: The ftb 5020 series: Technical documentation.
- Franz, S., Künzel, A., and Bruns, B. (2023). Innovative Messtechnik bei der Hangsicherung Heuberg (A 44). In *23. Symposium Brückenbau in Leipzig*.
- Hartog, A. H. (2017). *An Introduction to Distributed Optical Fibre Sensors*. CRC Press, Boca Raton.
- Henzinger, M. R., Schachinger, T., Lienhart, W., Buchmayer, F., Weilingner, W., Stefaner, R., Haberler-Weber, M., Haller, E.-M., Steiner, M., and Schubert, W. (2018). Fibre-optic supported measurement methods for monitoring rock pressure. *Geomechanics and Tunnelling*, 11(3):251–263.
- Hu, T., Hou, G., and Li, Z. (2020). The field monitoring experiment of the roof strata movement in coal mining based on dfos. *Sensors*, 20(5):1318.
- John, D. and Hoehn, K. (2024). Distributed fibre optic sensing for ground monitoring in underground hard rock mining. In *Deep Mining 2024: Proceedings of the 10th International Conference on Deep and High Stress Mining*, pages 391–402.
- Lopez-Higuera, J. M., Rodriguez Cobo, L., Quintela Incera, A., and Cobo, A. (2011). Fiber optic sensors in structural health monitoring. *Journal of Lightwave Technology*, 29(4):587–608.
- Minardo, A., Persichetti, G., Testa, G., Zeni, L., and Bernini, R. (2012). Long term structural health monitoring by brillouin fibre-optic sensing: a real case. *Journal of Geophysics and Engineering*, 9(4):64–69.
- Monsberger, C. M., Bauer, P., Buchmayer, F., and Lienhart, W. (2022). Large-scale distributed fiber optic sensing network for short and long-term integrity monitoring of tunnel linings. *Journal of Civil Structural Health Monitoring*, 12(6):1317–1327.
- Monsberger, C. M. and Lienhart, W. (2021). Distributed fiber optic shape sensing of concrete structures. *Sensors (Basel, Switzerland)*, 21(18).
- Naruse, H., Uehara, H., Deguchi, T., Fujihashi, K., Onishi, M., Espinoza, R., Guzman, C., Pardo, C., Ortega, C., and Pinto, M. (2007). Application of a distributed fibre optic strain sensing system to monitoring changes in the state of an underground mine. *Measurement Science and Technology*, 18(10):3202–3210.
- Nöther, N. (2010). *Distributed fiber sensors in river embankments: Advancing and implementing the Brillouin optical frequency domain analysis: Zugl.: Berlin, Techn. Univ., Diss., 2010*, volume 64 of *BAM-Dissertationsreihe*. Bundesanstalt für Materialforschung und -prüfung (BAM), Berlin.
- Pei, H.-F., Yin, J.-H., and Jin, W. (2013). Development of novel optical fiber sensors for measuring tilts and displacements of geotechnical structures. *Measurement Science and Technology*, 24(9):95202.
- Xie, J., Qu, Q., Zhu, W., Wang, X., Xu, J., Ning, S., Hou, T., and Luo, X. (2023). Distributed strain monitoring of overburden delamination propagation at a deep longwall mine. *International Journal of Rock Mechanics and Mining Sciences*, 171(2):105589.
- Ye, X. W., Su, Y. H., and Han, J. P. (2014). Structural health monitoring of civil infrastructure using optical fiber sensing technology: a comprehensive review. *TheScientificWorldJournal*, 14:652329.